





A Fully Automated Segmentation System of Positron Emission Tomography Studies

Albert Comelli^{1,2}(✉)  and Alessandro Stefano² 

¹ Fondazione Ri.MED, via Bandiera 11, 90133 Palermo, Italy
acomelli@fondazionerimed.com

² Institute of Molecular Bioimaging and Physiology,
National Research Council (IBFM-CNR), Cefalù, Italy

Abstract. In this paper, we present an automatic system for the brain metastasis delineation in Positron Emission Tomography images. The segmentation process is fully automatic, so that intervention from the user is never required making the entire process completely repeatable. Contouring is performed using an enhanced local active segmentation.

The proposed system is, at first instance, evaluated on four datasets of phantom experiments to assess the performance under different contrast ratio scenarios, and, successively, on ten clinical cases in radiotherapy environment.

Phantom studies show an excellent performance with a dice similarity coefficient rate greater than 92% for larger spheres. In clinical cases, automatically delineated tumors show high agreement with the gold standard with a dice similarity coefficient of $88.35 \pm 2.60\%$.

These results show that the proposed system can be successfully employed in Positron Emission Tomography images, and especially in radiotherapy treatment planning, to produce fully automatic segmentations of brain cancers.

Keywords: Active contour algorithm · Positron emission tomography imaging · Biological target volume · Segmentation

1 Introduction

Radiotherapy is often used to treat brain tumors otherwise inaccessible to conventional surgery. The classic and widespread approach to the identification of the volume to be treated is through the use of Magnetic Resonance Imaging (MRI). In particular, when soft-tissue contrast resolution needs to be high, as in brain malignancies, MRI is preferred over other approaches, e.g. computed tomography (CT). MRI has proved to be very efficient in reconstructing the anatomical properties of the investigated brain areas and for this reason, it has been almost the only diagnostic method employed for cancer delineation and treatment planning purposes [1–3]. Recently, the Positron Emission Tomography (PET) has been considered as a valuable source of information, in particular when the ¹¹C-labeled Methionine (MET) radio-tracer is considered. MET-PET conveys complementary information to the anatomical information derived from

MRI or CT, and under favorable conditions, it may even deliver higher performance [4]. For these reasons, the integration of PET imaging in radiotherapy planning represents a desirable step forward in the treatment of gliomas and brain metastases.

Several PET delineation approaches have been proposed so far [5–8], and for a comprehensive review, the interested reader may refer to Foster *et al.* [9] and references therein. In general, segmentation algorithms can be categorized as semi-automatic or automatic. When the 18F-fluoro-2-deoxy-d-glucose (FDG) radio-tracer is used, for example, the lesion must be initially highlighted by the operator. Indeed, for some healthy structures a high FDG uptake is normal; the brain is a typical example. As a result, segmentation methods in FDG PET studies are exclusively semi-automatic. However, MET radio-tracer shows great sensitivity and specificity for the discrimination of healthy versus brain cancer tissues, making automatic approaches feasible. In the present study we used MET-PET to deploy a fully automatic method to delineate brain cancer and metastases.

Starting from our previous study [10] where we proposed a semi-automatic tool to segment general oncological lesions in PET studies, we obtained a fully automatic and operator independent system for MET PET studies on the brain. In the proposed application, the system performs all segmentation step automatically by individuating an optimal, operator independent, initial mask located on an automatically selected PET slice. Once the initial region of interest (ROI) has been identified, it is fed to an enhanced local active contour segmentation algorithm. The objective function was adapted to PET imaging and designed in such a way that its minimum corresponds to the best possible segmentation. To assess the performance of the system and to verify its suitability as medical decision tool in radio-treatments, four phantom experiments, and ten patient studies were considered.

2 Materials and Methods

2.1 Overview of the Proposed System

The main subject of the present study is a fully automatic and operator independent system for brain cancer segmentation, to be used in radiotherapy treatments. While the following subsections will illustrate different components of the system and their validation, in this section we present a brief overview of the system design. The data hereby discussed comprise a total of four phantom experiments and ten oncological patients (Sects. 2.2 and 2.3, respectively). Data from phantoms were used to assess the performances of the delineation algorithm. Concerning the practical use of the system on clinical cases, in order to normalize the voxel activity and to take into account the functional aspects of the disease, the PET images were pre-processed into SUV images (Sect. 2.5). The first step is the automatic identification of the optimal combination of starting ROI and slice containing the tumor. Then, this information is input to the subsequent components of the system (Sect. 2.6). Once the ROI is identified, the corresponding mask is fed into the next step of the system, where the segmentation is performed combining a Local region-based Active Contour (LAC) algorithm, appropriately adapted to handle PET images. The resulting segmentation is then propagated to the adjacent slices using a slice-by-slice marching approach. Each time convergence criteria are met for a

specific slice, the corresponding optimal contour is propagated to the next, where the evolution is continued. Starting from the initial slice, the propagation is performed by contemporarily sweeping the data volume both upward and downward, until a suitable stopping condition, designed to detect a tumor-free slice, is met. Finally, the algorithm outputs a user independent Biological Tumor Volume (BTV). Detailed explanation of this task is provided in Sect. 2.7.

2.2 Phantom Studies

Four phantom experiments were used for preliminary assessment of the performance. The phantom is composed of an elliptical cylinder (minor axis = 24 cm, major axis = 30 cm, $h = 21$ cm) containing six different spheres (diameters: 10, 13, 17, 22, 28, and 37 mm) placed at 5.5 cm from the center of the phantom. The ratio between sphere and background radioactivity concentration ranged from 3:1 to 8:1. Performances were evaluated by grouping the results with respect to sphere diameters: small spheres, i.e. diameter smaller than 22 mm, and large spheres, with a diameter greater than 17 mm. This choice was motivated by the fact that large biases are introduced by the partial volume effect [11] in PET imaging.

2.3 Clinical Studies

Ten patients with brain metastases were retrospectively considered. These patients were referred to diagnostic PET/CT scan before Gamma Knife (Elekta, Stockholm, Sweden) treatment. Tumor segmentation was performed off-line without actually influencing the treatment protocol or the patient management. No sensitive patient data were accessed. As such, after all patients were properly informed and released their written consent, the institutional hospital medical ethics review board approved the present study protocol. Patients fasted 4 h before the PET examination, and successively were intravenously injected with MET. The PET/CT oncological protocol started 10 min after the injection.

2.4 PET/CT Acquisition Protocol

All acquisitions in this study were performed within the same hospital department and using the same equipment, a Discovery 690 PET/CT scanner (General Electric Medical Systems, Milwaukee, WI, USA). The PET protocol included a SCOUT scan at 40 mA, a CT scan at 140 keV and 150 mA (10 s), and 3D PET scans. The 3D ordered subset expectation maximization algorithm was used for the PET imaging. Each PET image consists of 256×256 voxels with a grid spacing of 1.17 mm^3 and thickness of 3.27 mm^3 . Consequently, the size of each voxel is $1.17 \times 1.17 \times 3.27 \text{ mm}^3$. Thanks to the injected PET radio-tracer, tumor appears as hyper-intense region. The CT scan was performed contextually to the PET imaging and used for attenuation correction. Each CT image consists of 512×512 voxels with size $1.36 \times 1.36 \times 3.75 \text{ mm}^3$.

2.5 Pre-processing of PET Dataset

Pre-processing PET images is mandatory for inter-patient and follow-up comparisons. Among PET quantification parameters, body-weight SUV is the most widely used in clinical routine. For this reason, it was embedded in our system. SUV is the ratio of tissue radioactivity concentration (RC) and injected dose (ID) at the time of injection, divided by body weight. The RC is calculated as the ratio between the image intensity and the image scale factor. The ID is calculated as the product between actual activity and dose calibration factor.

2.6 Interesting Uptake Region Identification

In order to obtain a fully automatic BTV segmentation, an initial ROI enclosing the tumor must be produced, obviously without any intervention by the operator. Therefore, the system identifies the PET slice containing the maximum SUV (SUV_{\max}) in the whole PET volume. By taking advantage of the great sensitivity and specificity of MET radiotracers in discriminating between healthy and tumor tissues, we can confidently assume that such SUV_{\max} resides inside the main lesion [12].

While this process takes place, an additional test is performed, in order to investigate the presence of isolated local maxima which may indicate metastases separated from the main lesion.

In the case that the presence of multiple (say “ n ”) independent anomalies are recognized, each one is independently processed. A different local maximum (SUV_{\max}^j , with $j = 1:n$) is identified for each lesion and, consequently, n regions are automatically identified. By design, the first identified lesion contains the global SUV_{\max} (i.e., SUV_{\max}^1).

Once the current slice with SUV_{\max}^j has been identified, an automatic procedure to identify the corresponding ROI starts. The SUV_{\max}^j voxel is used as target seed for a rough 2D segmentation based on the region growing (RG) method [13]. For each lesion, the obtained ROI represents the output of this preliminary step which is input to the next component of the system, where the actual delineation takes place. The latter is performed through an enhanced LAC segmentation algorithm. It is worth noting that the RG algorithm is used only to obtain a rough estimate of the tumor contour(s).

The same workflow is used to segment each metastasis independently, and the process is designed to carry on automatically. However, in case of multiple lesions the user will receive a warning message and if necessary, will be able to override the default behavior. In such a case, the algorithm can be paused, while the operator inspects the multiple metastases.

2.7 The Enhanced Local Active Contour Method

The model proposed by Lankton et al. [14] benefits of purely local edge based active contours and fully global region based active contours. At each point along a prominent intensity edge of the target, nearby points inside and outside the target will be modelled

well by the mean intensities within the local neighborhoods on either side of the edge. The contour energy to be minimized is defined as:

$$E = \oint_C \left(\int_{R_{in}} \chi_l(x, s)(I(x) - u_l(s))^2 dx + \int_{R_{out}} \chi_l(x, s)(I(x) - v_l(s))^2 dx \right) ds \quad (1)$$

- R_{in} and R_{out} represent the regions inside and outside the curve C
- s represents the arc length parameter of C
- χ represents the characteristic function of the ball of radius l (local neighborhood) centered around a given curve point $C(s)$
- I represents the intensity function of the image to be segmented
- $u_l(s)$ and $v_l(s)$ denote the local mean image intensities within the portions of the local neighborhood $\chi_l(x, s)$ inside and outside the curve respectively (within R_{in} and R_{out}).

These neighborhoods are defined by the function χ , the radius parameter l , and the position of the curve C . Note that the function $\chi_l(x, s)$ evaluates to 1 in a local neighborhood around each contour point $C(s)$ and 0 elsewhere. The contour C then divides each such local region into interior and exterior local pixels in accordance with the contour's rule to segment the domain of I .

Beyond the optimal identification of the starting slice containing the lesion, and, consequently, the identification of an initial operator independent mask for LAC segmentation (see Sect. 2.6) further improvements have been introduced in the LAC algorithm. In the following we summarize part of the method, described in [10]. To incorporate metabolic information, the intensity function I in (1) is replaced by the SUV, and $u_l(s)$ and $v_l(s)$ denote the local mean SUV intensities within the portions of the local neighborhood $\chi_l(x, s)$ inside and outside the curve. The shape of the contour C then divides each such local region into interior local points and exterior local points in accordance with the contour's segmentation of the SUV. The local means are specified as the ratios of $S_{I_l}(s)$, $S_{E_l}(s)$, $A_{I_l}(s)$, and $A_{E_l}(s)$ which represent the local sums of SUV intensities and the areas of their respective portions of the local neighborhood $\chi_l(x, s)$ inside and outside the curve. More precisely, the local interior region may be expressed as $R_{in} \cap \chi_l(x, s)$ and local exterior region as $R_{out} \cap \chi_l(x, s)$.

$$u_l(s) = \frac{S_{I_l}(s)}{A_{I_l}(s)}, \quad v_l(s) = \frac{S_{E_l}(s)}{A_{E_l}(s)}$$

$$S_{I_l}(s) = \int_{R_{in}} \chi_l(x, s) SUV(x) dx, \quad S_{E_l}(s) = \int_{R_{out}} \chi_l(x, s) SUV(x) dx$$

$$A_{I_l}(s) = \int_{R_{in}} \chi_l(x, s) dx, \quad A_{E_l}(s) = \int_{R_{out}} \chi_l(x, s) dx$$

$$\chi_l(x, s) = \begin{cases} 1 & \text{when } x \in l - \text{Ball}(C(s)); \\ 0 & \text{otherwise;} \end{cases}$$

Once the ROI encircling the highest radio-tracer uptake area has been automatically identified (previous section), the resulting mask is used to initiate parallel segmentations on the neighboring slices above and below. Subsequently, for all the other slices in both directions, we similarly use the segmentation results of the previous slices as the initial mask inputs. The LAC method is inherently capable of locally widening or tightening where necessary when the contour is propagated from slice to slice. Since, this behavior is driven by the image properties rather than by an inherent knowledge of whether the cancer is present, a stopping criterion is necessary to prevent the LAC algorithm from misbehaving, or even diverging, when it reaches a slice where the cancer is absent (i.e. when there is nothing to be segmented).

Therefore, a fully automatic stopping condition is implemented. For the slice under consideration, at each point on the cancer edge, nearby points inside and outside the cancer must have a different local mean SUV. If the cancer is present, a positive difference between background and foreground intensity must occur, and consequently the algorithm can safely proceed with the next neighboring slice. When the system encounters a slice where the local mean $v_1(s)$ on R_{out} is greater or equal to the local mean SUV $u_1(s)$ on R_{in} , which is the opposite of what is expected, the slice is recognized as cancer-free and the slice-to-slice propagation is terminated in that direction. In this way, one slice at a time, the BTV is generated. Finally, the segmentation process is automatically stopped, thereby avoiding the need for any user intervention.

2.8 Framework for Performance Evaluation

Overlap-based and spatial distance-based metrics are considered to determine the accuracy achieved by the automatic segmentation system against the gold-standard [15]. In particular, the formulations of dice similarity coefficient (DSC), and Hausdorff distance (HD) are used.

DSC measures the spatial overlap between the reference volume and the segmentation system: a DSC value equal to 100% indicates a perfect match between two volumetric segmentations, while $DSC = 0\%$ indicates no overlap. Nevertheless, overlap-based metrics are not well suited for small anomalies. For this reason, distance-based metrics are preferable, especially when the boundary segmentation is critical, such as in BTV delineation for RTP. In particular, HD is used to measure the most mismatched boundary voxels between automatic and manual BTV: small HD means an accurate segmentation, while a large HD is synonymous of poor accuracy.

Finally, the performance of the proposed method is compared to other state of the art BTV segmentation methods: the original LAC method [17], the RG method [18], the enhanced RW method such as described in [19], and the FCM clustering method [20].

3 Results

3.1 Phantom Studies

Performance results from phantom experiments were divided considering small and large spheres, in four independent cases, each carried out with different signal ratios.

The accuracy improved for all spheres, regardless of their volume, when the signal ratio increased. In general, due to the partial volume effect, the separation of small targets from the background is very challenging, and the difficulty increases in condition of low signal contrast. The sphere volumes are underestimated with more false negatives than false positives. The dice similarity coefficient (DSC) rate is $77.51 \pm 3.46\%$ and the Hausdorff distance (HD) is 1.12 ± 0.15 voxels. For the spheres with a diameter greater than 17 mm, excellent performances are obtained with a DSC rate greater than 92% ($HD = 1.06 \pm 0.09$). The mean difference between segmented and actual volumes is positive (the sphere volumes are overestimated); larger margins can help to prevent the extension of tumor infiltration.

The performance of the system was compared to other state of the art PET image segmentation methods. In particular, the original LAC [17], the RG [18], the RW [19], and the FCM [20] methods have been used for comparison. Table 1 summarizes the results and shows that this automatic segmentation outperforms the methods tested for comparison for all the considered cases.

Table 1. DSC and HD values for the proposed method and other state of the art PET image segmentation methods.

	DSC	HD (voxels)
Our system	$84.79 \pm 8.00\%$	1.09 ± 0.12
Original LAC	$82.55 \pm 7.56\%$	1.44 ± 0.55
RW	$82.12 \pm 8.78\%$	1.22 ± 0.43
RG	$79.01 \pm 9.34\%$	1.67 ± 0.57
FCM	$77.13 \pm 8.79\%$	1.68 ± 0.49

3.2 Clinical Studies

The performance of the presented system is investigated considering ten metastases against the ground truth provided by three expert operators. In clinical cases, the histopathology analysis is unavailable after the gamma knife treatment. For this reason, the manual delineation performed by expert clinicians is a commonly accepted substitute for ground truth to assess the clinical effectiveness and feasibility of PET delineation methods. Consequently, manual segmentations performed by three experts are used to define a consolidated reference using STAPLE algorithm [16]. This simultaneous ground truth estimation tool combines a collection of segmentations into a single and consolidated ground truth segmentation. It computes a probabilistic estimate of the true segmentation estimating an optimal combination of the segmentations. This algorithm is formulated as an instance of the expectation maximization (EM).

Differently from the phantom studies, no discussion of the tumor volumes is provided here, mostly because all considered BTVs are greater than 2.5 ml (lesions with a sphere-equivalent diameter greater than 17 mm). In particular, tumor volumes ranged from 2.69 ml to 20.49 ml (mean \pm std = 7.08 ± 5.81 ml). The ratio between lesion and

background radioactivity concentration ranged from 2.76:1 to 7.40:1 (mean \pm std = 3.88:1 \pm 1.45:1). These values are included in the range of the phantom experiments used for preliminary performance testing. For this reason, although phantom studies don't replicate all the properties of real lesions, they represent a useful tool to assess performances across different segmentation methods.

Table 2 summarizes the comparison between this automatic segmentation and the original LAC and RW approaches. Since LAC and RW outperformed RG, and FCM methods on the phantom experiments, the latter algorithms were not considered in patient studies. The automatic algorithm performed better than LAC and RW methods minimizing the difference between references and automated BTVs.

Table 2. DSCs and HDs using the proposed system, original LAC and RW methods.

	DSC	HD
Our system	88.35 \pm 2.60%	1.42 \pm 0.57
Original LAC	83.77 \pm 8.53%	2.97 \pm 0.68
RW	87.01 \pm 5.16%	1.38 \pm 0.74

Figure 1 reports the comparison between the proposed segmentations and the gold-standards.

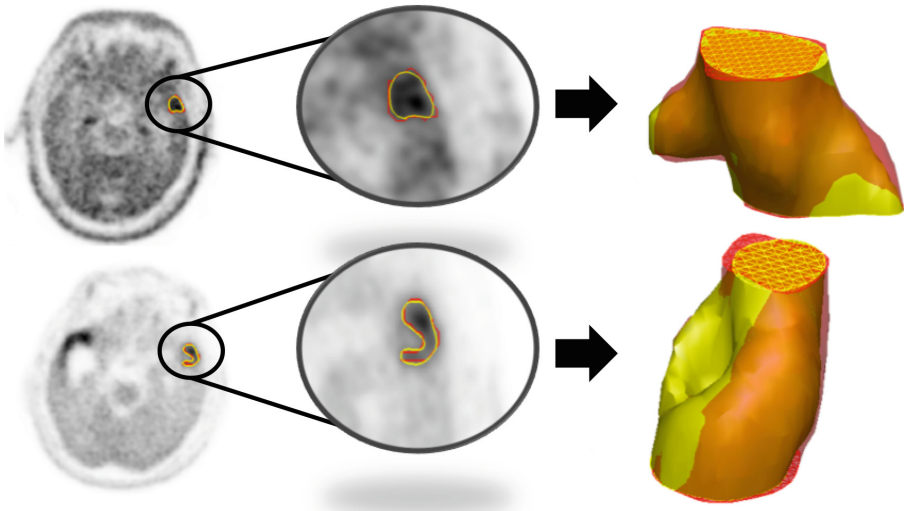


Fig. 1. Examples of automatic segmentations. The retrieved segmentations and the gold standards are shown in red and yellow, respectively. (Color figure online)

4 Discussion

In this study, a complex, semi-automatic system featuring an enhanced LAC algorithm purposely adapted to the PET imaging was further adapted to achieve the fully automatic BTV segmentations of brain cancers. The fully automatic approach leverages on the fact that MET-PET is capable of selectively highlight the ill regions of the brain, so avoiding false positives commonly encountered in other anatomic regions (e.g. as in FDG-PET studies). An automatic and operator-independent ROI is generated around the tumor(s) and used as input to an enhanced LAC algorithm. Then, the LAC performs the BTV delineation. The BTV is built by a slice-by-slice marching approach where the segmentation is performed on subsequent slices. In principle, segmentation through the evolution of a full 3D surface would be preferable. Indeed, while on the one hand we are currently investigating such a 3D approach, on the other hand, the present work moves an important step toward 3D data segmentation improving upon the model proposed by Lankton et al. [14] considering the issue of the PET slices thickness (3.27 mm^3) far greater than planar resolution (1.17 mm^3) which partially justifies the 2D approach. As a final remark, a fully automatic stop condition is provided. In this way, the proposed system produces segmentation results which are completely independent by the user.

Performance of the automatic system has been obtained by phantom studies consisting of hot spheres in a warm background. Nevertheless, phantom experiments cannot replicate all the aspects of a real clinical case but they represent a useful way to assess common performances across different algorithms. DSC greater than 92% for the larger spheres confirm better results in minimizing the difference between reference and automated BTVs than the other state-of-the-art algorithms. We would like to emphasize that original algorithms for both enhanced RW and original LAC methods [17, 19] were optimized for MET-PET brain metastases [10, 12]. Concerning RG and FCM methods, we used the source codes available on the web, and we adapted it to our PET dataset.

In patient studies, since radiotherapy treatment alters the cancer morphology over time, histopathology cannot provide a reliable ground truth. Consequently, manual delineation by experts, although it may differ between operators (for example, radiotherapy experts tend to draw larger boundaries than nuclear medicine physicians), is often used as surrogate gold-standard. In this study, we used manual delineations from three experts. To overcome the issue of differences in the manual delineations, a consolidated reference was built [16] and then used to assess the feasibility of the automatic segmentation. PET/CT data from ten patients before Gamma Knife treatment were considered. Results show that the proposed approach can be considered clinically feasible and could be used to extract PET parameters for therapy response evaluation purpose and to assist the BTV delineation during stereotactic radiosurgery treatment planning avoiding cancer recurrence. Finally, further investigations will be carried out to assess the usefulness to introduce in the segmentation a PET tissue classifier capable of influencing the local active contour toward what would be the segmentation performed by a human operator [21–25].

Acknowledgments. Authors would like to thank Prof. Anthony Yezzi, Dr. Samuel Bignardi, Dr. Giorgio Russo, MD. Maria Gabriella Sabini, and MD. Massimo Ippolito for their crucial support in the management of the proposed study.

References

1. Comelli, A., Bruno, A., Di Vittorio, M.L., et al.: Automatic Multi-seed Detection for MR Breast Image Segmentation, pp. 706–717. Springer, Cham (2017)
2. Chandarana, H., Wang, H., Tijssen, R.H.N., Das, I.J.: Emerging role of MRI in radiation therapy. *J. Magn. Reson. Imaging* **48**, 1468–1478 (2018). <https://doi.org/10.1002/jmri.26271>
3. Agnello, L., Comelli, A., Ardizzone, E., Vitabile, S.: Unsupervised tissue classification of brain MR images for voxel-based morphometry analysis. *Int. J. Imaging Syst. Technol.* (2016). <https://doi.org/10.1002/ima.22168>
4. Astner, S.T., Dobrei-Ciuchendea, M., Essler, M., et al.: Effect of ¹¹C-methionine-positron emission tomography on gross tumor volume delineation in stereotactic radiotherapy of skull base meningiomas. *Int. J. Radiat. Oncol. Biol. Phys.* **72**, 1161–1167 (2008). <https://doi.org/10.1016/j.ijrobp.2008.02.058>
5. Comelli, A., Stefano, A., Bignardi, S., et al.: Active contour algorithm with discriminant analysis for delineating tumors in positron emission tomography. *Artif. Intell. Med.* **94**, 67–78 (2019). <https://doi.org/10.1016/J.ARTMED.2019.01.002>
6. Comelli, A., Stefano, A., Russo, G., et al.: K-nearest neighbor driving active contours to delineate biological tumor volumes. *Eng. Appl. Artif. Intell.* **81**, 133–144 (2019). <https://doi.org/10.1016/j.engappai.2019.02.005>
7. Hatt, M., Cheze Le Rest, C., Albarghach, N., et al.: PET functional volume delineation: a robustness and repeatability study. *Eur. J. Nucl. Med. Mol. Imaging* **38**, 663–672 (2011). <https://doi.org/10.1007/s00259-010-1688-6>
8. Berthon, B., Spezi, E., Galavis, P., et al.: Toward a standard for the evaluation of PET-Auto-Segmentation methods following the recommendations of AAPM task group No. 211: Requirements and implementation. *Med Phys.* (2017). <https://doi.org/10.1002/mp.12312>
9. Foster, B., Bagci, U., Mansoor, A., et al.: A review on segmentation of positron emission tomography images. *Comput. Biol. Med.* **50**, 76–96 (2014). <https://doi.org/10.1016/j.compbiomed.2014.04.014>
10. Comelli, A., Stefano, A., Russo, G., et al.: A smart and operator independent system to delineate tumours in Positron Emission Tomography scans. *Comput. Biol. Med.* (2018). <https://doi.org/10.1016/J.COMPBIOMED.2018.09.002>
11. Soret, M., Bacharach, S.L., Buvat, I.I.: Partial-volume effect in PET tumor imaging. *J. Nucl. Med.* **48**, 932–945 (2007). <https://doi.org/10.2967/jnumed.106.035774>
12. Stefano, A., Vitabile, S., Russo, G., et al.: A fully automatic method for biological target volume segmentation of brain metastases. *Int. J. Imaging Syst. Technol.* **26**, 29–37 (2016). <https://doi.org/10.1002/ima.22154>
13. Stefano, A., et al.: An automatic method for metabolic evaluation of gamma knife treatments. In: Murino, V., Puppo, E. (eds.) *ICIAP 2015. LNCS*, vol. 9279, pp. 579–589. Springer, Cham (2015). https://doi.org/10.1007/978-3-319-23231-7_52
14. Lankton, S., Nain, D., Yezzi, A., Tannenbaum, A.: Hybrid geodesic region-based curve evolutions for image segmentation. In: *Proceedings of the SPIE 6510, Medical Imaging 2007: Physics of Medical Imaging*, 16 March 2007, p. 65104U (2007). <https://doi.org/10.1117/12.709700>
15. Udupa, J.K., Leblanc, V.R., Zhuge, Y., et al.: A framework for evaluating image segmentation algorithms. *Comput. Med. Imaging Graph.* **30**, 75–87 (2006). <https://doi.org/10.1016/j.compmedimag.2005.12.001>
16. Warfield, S.K., Zou, K.H., Wells, W.M.: Simultaneous truth and performance level estimation (STAPLE): an algorithm for the validation of image segmentation. *IEEE Trans. Med. Imaging* **23**, 903–921 (2004). <https://doi.org/10.1109/TMI.2004.828354>

17. Lankton, S., Nain, D., Yezzi, A., Tannenbaum, A.: Hybrid geodesic region-based curve evolutions for image segmentation. 65104U (2007). <https://doi.org/10.1117/12.709700>
18. Day, E., Betler, J., Parda, D., et al.: A region growing method for tumor volume segmentation on PET images for rectal and anal cancer patients. *Med. Phys.* **36**, 4349–4358 (2009). <https://doi.org/10.1118/1.3213099>
19. Stefano, A., Vitabile, S., Russo, G., et al.: An enhanced random walk algorithm for delineation of head and neck cancers in PET studies. *Med. Biol. Eng. Comput.* **55**, 897–908 (2017). <https://doi.org/10.1007/s11517-016-1571-0>
20. Belhassen, S., Zaidi, H.: A novel fuzzy C-means algorithm for unsupervised heterogeneous tumor quantification in PET. *Med. Phys.* **37**, 1309–1324 (2010). <https://doi.org/10.1118/1.3301610>
21. Licari, L., et al.: Use of the KSVM-based system for the definition, validation and identification of the incisional hernia recurrence risk factors. *Il Giornale di chirurgia* **40**(1), 32–38 (2019)
22. Agnello, L., Comelli, A., Vitabile, S.: Feature dimensionality reduction for mammographic report classification. In: Pop, F., Kołodziej, J., Di Martino, B. (eds.) *Resource Management for Big Data Platforms*. CCN, pp. 311–337. Springer, Cham (2016). https://doi.org/10.1007/978-3-319-44881-7_15
23. Comelli, A., et al.: A kernel support vector machine based technique for Crohn's disease classification in human patients. In: Barolli, L., Terzo, O. (eds.) *CISIS 2017. AISC*, vol. 611, pp. 262–273. Springer, Cham (2018). https://doi.org/10.1007/978-3-319-61566-0_25
24. Comelli, A., Stefano, A., Benfante, V., Russo, G.: Normal and abnormal tissue classification in pet oncological studies. *Pattern Recogn. Image Anal.* **28**, 121–128 (2018). <https://doi.org/10.1134/S1054661818010054>
25. Comelli, A., Agnello, L., Vitabile, S.: An ontology-based retrieval system for mammographic reports. In: *Proceedings of IEEE Symposium Computers and Communication* (2016). <https://doi.org/10.1109/ISCC.2015.7405644>